Title: A Comparison of Square-Wave Voltammetry Models to Determine the Number of Electrons Exchanged in Metal Deposition

Author Names and Affiliations:
Corresponding author: Ranon Fuller[a], ranongf@byu.edu
Tyler Williams[a], wtylerb@byu.edu
Mark Schvaneveldt[a], mschvane@byu.edu
Devin Rappleye[a], devin_rappleye@byu.edu

[a] Department of Chemical Engineering, Engineering Building 330, Brigham Young University, Provo, UT 84602, USA

 https://doi.org/10.1016/j.electacta.2022.140220

Abstract

A comparison of square-wave voltammetry models for calculating the number of electrons exchanged in a metal deposition reaction. Experiments were conducted for silver deposition on platinum in an aqueous HNO_3 solution and for nickel and lanthanum deposition on platinum in molten LiCl. Diffusion coefficients for Ni^{2+} and La^{3+} in LiCl at 700°C are calculated. Accuracy of soluble-soluble models versus a soluble-insoluble model is discussed. A simple method for determining the number of electrons exchanged under the constraint of well-compensated ohmic drop is proposed and evaluated.

Keywords

Metal deposition, molten salt, square-wave voltammetry

Funding

This research did not receive any specific grant from funding agencies in the public, commercial, or not-for-profit sectors.

1. Introduction

Square-wave voltammetry (SWV) is an extremely useful technique for analyzing electrochemical reactions. Its ability to minimize background current makes it ideal for detecting species at low concentrations and isolating the behavior of a single reaction in a mixed solution of many reacting species. SWV can also help characterize unknown compounds in solution by identifying the electrochemical potential and number of electrons exchanged in a reaction. These features make SWV an invaluable tool for the detection and identification of corrosion products and other contaminants in aqueous and molten salt media, such as those used in concentrated solar power, thermal energy storage, pyroprocessing, and the development of molten salt nuclear reactors.

 https://doi.org/10.1016/j.electacta.2022.140220

Although theoretical models for soluble-soluble reactions are well established, little work has been done to validate these models for metal deposition reactions. Many recent publications [1–10] on square-wave voltammetry feature a version of Barker's or Aoki et al.'s soluble-soluble reaction model to describe the electrochemical response of metal deposition [11,12]. This application is fundamentally incorrect and predicts the right number of electrons only by chance since metal deposition typically involves one soluble species and one insoluble solid species [13]. In 2013, Fatouros and Krulic proposed a model to explain the behavior of metal deposition reactions and demonstrated its validity for silver deposition on gold in an acidic, aqueous environment [13].

In this work, Fatouros and Krulic's model is tested against Barker's and Aoki et al.'s model in both aqueous and molten salt environments and for reactions in which one, two, and three electrons are exchanged. In addition to testing the accuracy of these two models, a simplified version of Fatouros and Krulic's model is proposed that introduces minor additional error under the condition of well-compensated ohmic drop. This model (referred to as the "IR-compensated Fatouros and Krulic" model) reduces the work required to calculate the number of electrons exchanged by only requiring knowledge of the temperature and SWV peak width. This IR-compensated version is more practical and may be easily applied in the real-time identification of unknown reacting species for commercial and research applications.

2. Theory

Barker (1956) was the first to report a relationship between the peak width at half height for square-wave polarography [11]:

 https://doi.org/10.1016/j.electacta.2022.140220

$$W_{1/2} = 3.52\frac{RT}{nF} \quad (1)$$

where $W_{1/2}$ is the peak width at half height, R is the gas constant, T is temperature, n is the number of electrons exchanged in the reaction, and F is Faraday's constant. This model was applied under the assumption of a reversible redox reaction where both oxidized and reduced species are soluble in either the electrode or in the solution and the peak-to-peak square-wave amplitude (ΔE) is much smaller than RT/nF [11].

Ramaley and Krause (1969) derived a similar relationship between peak width at half height for square-wave voltammetry and compared it to that obtained by Baker (1956) with extremely good agreement. They found that under the constraint of small square-wave distortion, Barker's relationship for peak width at half height may be used for square-wave voltammetry with a stationary electrode [14,15]. Their theory was again derived under the assumptions of a reversible reaction between two species that are soluble in either the solution or the electrode.

Aoki et al. (1986) developed a more complex mathematical model to describe this relationship between peak width at half height [12]:

$$W_{1/2} = \left(\frac{RT}{nF}\right)\left(3.53 + 3.46\frac{\xi_{SW}^2}{\xi_{SW} + 8.1}\right) \quad (2)$$

where:

$$\xi_{SW} = \frac{nF\Delta E}{RT} \quad (3)$$

and ΔE again is the square-wave amplitude. Their model is derived under the assumptions: "(a) the electrochemical reaction takes place so rapidly that the Nernst equation holds at the electrode surface; (b) the oxidized and the reduced species are transported in the solution only by

 https://doi.org/10.1016/j.electacta.2022.140220

diffusion; (c) the diffusion coefficients of both species have a common value, D; and (d) only the reduced species is initially present in the solution" [12].

It should be noted that Equation (2) reduces to an equation very similar to Equation (1) as ΔE approaches zero. They become within 5% of each other when ΔE is approximately 17 mV for n=1, 8.6 mV for n=2, and 5.7 mV for n=3 at 25°C.

Likely due to nucleation effects of depositing a metal on a foreign substrate (i.e., the electrode), the SWV reduction peak for metal deposition is not an ideal bell-shape. In these cases published literature often takes the second half of the peak width and doubles it in attempt to get a more 'accurate' value for $W_{1/2}$ [1,2,4,6,16]. In this paper the same method will be applied when using equations (1) and (2) for comparative purposes.

Fatouros and Krulic (2013) derived an original expression using SWV to determine the number of electrons exchanged in an electrochemical reaction where the oxidized species is soluble in solution, but the reduced species is not [13]:

$$w_2 = \frac{W_2 RT}{nF} \tag{4}$$

where w_2 is the width of the second half of the deposition peak at half height, starting at the peak potential as shown in Figure 1, and $\mathcal{W}_2$ is given by the expression:

$$\mathcal{W}_2 = 0.37\chi^{-0.5} + 0.45\chi^{0.11} + (0.26 + 0.01\chi)\rho \tag{5}$$

χ and ρ in Equation (5) are the following dimensionless parameters:

$$\chi = \frac{C_{ox}^{*}\sqrt{D_{ox}\Delta t}}{\Gamma_1} \tag{6}$$

 https://doi.org/10.1016/j.electacta.2022.140220

$$\rho = \frac{n^2 F^2 A R_u C_{ox}^* \sqrt{D_{ox}}}{RT\sqrt{\Delta t}} \quad (7)$$

where C_{ox}^* is the concentration of the oxidized metal ion in the bulk solution, D_{ox} is the diffusion coefficient of the oxidized species, Δt is the pulse duration (equal to $1/2f$ where f is the frequency), as shown in Figure 2, Γ_1 is the surface concentration of the reduced species for which its activity becomes 1, A is the electrode area, and R_u is the uncompensated resistance in the cell. In their derivation they assumed: a planar electrode, excess supporting electrolyte, that the specific adsorption of metal ions in the underpotential range is the first step of the electrodeposition process, and the reaction is diffusion controlled [13].

Fatouros and Krulic state that "in order to obtain voltammograms of sufficient resolution and avoid long recording times which could affect the current because of the finite spread of the diffusion layer, especially in the presence of high metal ion concentration," they give the following operation guidelines for square-wave amplitude and step potential:

$$\frac{-0.23RT}{nF} < \Delta E_s < \frac{-0.04RT}{nF} \quad (8)$$

$$\frac{0.8RT}{nF} < \Delta E < \frac{4.7RT}{nF} \quad (9)$$

where ΔE_s is the step potential and ΔE is again the peak-to-peak amplitude, as shown in Figure 2.

Fatouros and Krulic observed that as Δt approaches zero, $\mathcal{W}_2$ approaches 0.7. Thus, they determined that for $\chi > 3.7$, Equation (5) may be approximated as:

 https://doi.org/10.1016/j.electacta.2022.140220

$$\mathcal{W}_2 = 0.7 + 0.3\rho \tag{10}$$

In this paper, Equation (10) will be referred to as the "Fatouros and Krulic truncated" model (F&K Truncated for short). It then follows that when the ohmic drop in solution is well compensated, R_u will become small and therefore ρ will be small. For example, when ρ = 0.1, resistance contributes less than 5% to $\mathcal{W}_2$. Under these conditions it may be appropriate to use the following approximation while introducing only a small amount of error:

$$\mathcal{W}_2 = 0.7 \tag{11}$$

Equation (11) will be referred to as the "IR-compensated Fatouros and Krulic" model (IR-F&K for short).

Although Fatouros and Krulic's theory was developed for planar electrodes, cylindrical electrodes may be approximated as planar with less than 5% error if the following relation holds [17]:

$$\frac{D_{ox}\Delta t}{r^2} \leq 3 \times 10^{-3} \tag{12}$$

where r is the radius of the cylindrical electrode.

To calculate a value for the diffusion coefficient of an oxidized species in solution the Berzins-Delahay relationship is used. In 1953, Berzins and Delahay derived a model for how the peak current (i_p) varies as a function of the square root of the scan rate (ν) for a reversible deposition reaction in cyclic voltammetry [18]:

$$i_p = 0.6105AC_{ox}^{*}\sqrt{\frac{(nF)^3 D_{ox}\nu}{RT}} \tag{13}$$

 https://doi.org/10.1016/j.electacta.2022.140220

All other variables take the same meaning as defined above. Reversibility in electrochemical reactions is characterized by fast kinetics relative to the mass transport of reactants to the electrode surface, such that Nernstian behavior can be assumed at the electrode. Thus, metal deposition reactions are considered reversible for low scan rates. This relationship proposed by Berzins and Delahay may also provide criteria for determining reversibility. As shown by Equation (13), for a given reaction in the reversible region, the peak current (i_p) varies linearly with the square root of the scan rate $(\sqrt{\nu})$. Additionally, the peak potential (E_p) is independent of the scan rate. These two relationships may be used to determine reversibility [17].

To calculate Γ_1 used in Equation (6), the following equation may be used:

$$\Gamma_1 = \frac{Q_m}{nF} \tag{14}$$

where Q_m is the theorietical charge density given by [19]:

$$Q_m = \frac{ze}{(2r_a)^2} \tag{15}$$

where z is the valence charge of the metal, e is the electronic charge, and r_a is the atomic radius.

3. Experimental Methods

To compare each mathematical model's ability to accurately calculate the number of electrons exchanged in a metal deposition reaction, three sets of experiments were completed: the one-electron exchange of silver deposition on platinum in an aqueous, 1 M nitric acid environments; the two-electron exchange of nickel deposition on tungsten in molten LiCl; and the three-electron exchange of lanthanum deposition on tungsten in molten LiCl. These three systems were chosen as examples of one, two, and three-electron exchange reactions respectively, to use for comparing the accuracy of SWV models. 1 M nitric acid was chosen as the bath formulation for

 https://doi.org/10.1016/j.electacta.2022.140220

silver deposition to replicate the original results of Fatouros and Krulic [13]. Nickel and lanthanum deposition in molten LiCl were chosen to extend the validation of these models from aqueous solutions and single-electron exchange reactions to molten salts and multi-electron exchange reactions. LiCl was chosen as the salt for both nickel and lanthanum deposition due to its wide electrochemical window and relatively low melting point. The concentration of analyte in each solution was selected to capture a broad range of SWV frequencies where equations (10) and (11) could be applied by maintaining $\chi > 3.7$ and $\rho < 0.1$ based on equations (6) and (7), respectively.

The potentiostat used for both aqueous and molten salt experiments were PGSTAT302N models with an FRA32M module, produced by Metrohm. To compensate for ohmic resistance effects on potential measurements, the potentiostat's built-in real-time compensation method was used.

3.1 $AgNO_3$ in 1 M HNO_3

The solution was composed of 0.027 M $AgNO_3$ and 1 M HNO_3 in deionized water. The working electrode (WE) was a 5 mm diameter Pt disk electrode (Pine Research Instrumentation, AFE3T050PT). The counter electrode (CE) was a 0.02 in diameter Nb wire coated with 0.0001" of Pt (Anomet) and the reference electrode (RE) was a 0.5 mm diameter silver wire (99.9%, Alfa-Aesar, 41390) quasi-reference electrode. The temperature of this experiment was measured to be 23.1°C. The ohmic drop in this experiment was found to be 7.24 Ω as measured by electronic impedance spectroscopy (EIS) at a potential of 0.0 V verses a Ag/AgCl reference electrode in the range of 10 Hz to 1,000,000 Hz, and amplitude of 0.01 V, and a frequency step of 10 points per decade. Measurements were taken with a range of IR compensations between 90-99.9%. The working electrode area for this experiment was 0.785 cm^2.

 https://doi.org/10.1016/j.electacta.2022.140220

To test the accuracy of equations (1), (2), (5), (10), and (11), a series of square-wave voltammetry measurements at varying frequencies were conducted.

3.2 $NiCl_2$ and $LaCl_3$ in Molten LiCl

Molten LiCl experiments were performed in an LC Technology Solutions LC-300-DS glovebox under an argon atmosphere. H_2O and O_2 levels were maintained at 0 ppm and under 10 ppm, respectively. Prior to use, the lithium chloride was dried in a vacuum oven at 110°C for 6 hours followed by 186°C for 18 hours [20], then premelted and cooled in the argon glovebox. Ultra-dry $NiCl_2$ (99.9%, Alfa-Aesar, 35713) and $LaCl_3$ (99.9%, Alfa-Aesar, 35702) was used without further drying.

All molten salt experiments were performed in alumina crucibles that had been previously cleaned with aqua regia to remove contaminants, then dried at 248.8°C under vacuum for >12 hours, and then heated to 900°C inside of the argon glovebox. The WE for these experiments was a 1.5 mm tungsten rod (99.95%, Alfa-Aesar, 42233), the CE was a 3.175 mm tungsten rod (99.95%, Alfa-Aesar, 10407), and the RE was a 1 mm tungsten wire quasi-reference electrode (99.95%, Alfa-Aesar, 10411). Figure 3 shows a cross-section sketch of the experimental setup. As shown in this figure, all experiments were surrounded by a grounded nickel tube inside the tube furnace to reduce noise due to electromagnetic fields. The temperature was maintained at 701°C for the nickel experiments and 698°C for the lanthanum experiments.

To calculate values for the diffusion coefficients of Ni^{2+} and La^{3+} in molten LiCl, a series of cyclic voltammetry (CV) measurements were performed at varying scan rates. From this data

 https://doi.org/10.1016/j.electacta.2022.140220

and Equation (13), the reversibility region and diffusion coefficients were determined. All diffusion coefficient experiments were done with an IR compensation of 85%. After completion of CV measurements, square-wave voltammetry measurements with varying frequencies and a range of IR compensations were performed, similar to the measurements of $AgNO_3$ in 1 M HNO_3.

For the experiments with nickel, the composition of $NiCl_2$ in the salt was found to be 0.419 weight percent (wt.%), as measured by ICP-MS. The working electrode area was measured to be 0.66 cm^2 by physical inspection of the adhering salt after allowing time for wetting. The ohmic drop was found to be 0.122 Ω as measured by EIS at a potential of -0.015 V verses a tungsten wire pseudo reference electrode in the range of 100 Hz to 100,000 Hz, and amplitude of 0.01 V, and a frequency step of 10 points per decade.

For the experiments with lanthanum, the composition of $LaCl_3$ was found to be 0.433 wt.% as measured by ICP-MS. The working electrode area was measured to be 0.66 cm^2. The ohmic drop was found to be 0.118 Ω as measured by EIS at a potential of -1.5 V verses a tungsten wire pseudo reference electrode in the range of 100 Hz to 100,000 Hz, and amplitude of 0.01 V, and a frequency step of 10 points per decade.

4. Results and Discussion

4.1 Ag Deposition on Pt

To gather data for comparing models to calculate the number of electrons exchanged in silver deposition, square-wave voltammetry measurements for silver deposition on platinum were conducted over a frequency range of 0.1-10 Hz. Table 1 shows the experimental parameters that

 https://doi.org/10.1016/j.electacta.2022.140220

were operated at compared to those recommended in Equations (8) and (9) for this experiment. As seen in this table, the experiment was well within the limits suggested.

Table 1: Experimental and recommended step potential and amplitude potential for silver deposition

	ΔE_s/V	$\Delta E/V$
Recommended Range [13]	-0.0059 to -0.0010	0.020 to 0.120
Experimental Parameters	-0.003	0.1

The results of the SWV experiments with silver are reported in Figure 4. In this figure the second half of the peak width at half height (w_2) is graphed as a function of the square root of the pulse duration $(\Delta t^{1/2})$. Along with the experimental data, the w_2 is graphed as predicted by each of equations (1), (2), (5), (10), and (11) for comparison. As predicted by the theory, w_2 approaches a constant value with increasing $\Delta t^{1/2}$.

As shown in Figure 4, three sets of measurements were performed at different IR compensations: 90%, 95%, and 99.9%. Since the total IR drop was found to be 7.24 Ω, these percentages correspond to an IR compensation of 6.52 Ω, 6.88 Ω, and 7.23 Ω respectively. This figure also shows that all three Fatouros and Krulic models appear to have strong agreement with the experimental data at lower frequencies while the soluble-soluble models are far from correct.

As predicted by Fatouros and Krulic, w_2 theoretically will approach a minimum value as $\Delta t^{1/2}$ increases. The skew in the data at high values of $\Delta t^{1/2}$ is thought to be a result of surface area

 https://doi.org/10.1016/j.electacta.2022.140220

growth. Because of these competing factors, the lowest value of w_2 in each data set was chosen as the representative value for that experiment. These data along with their associated χ values are reported in Table 2. The Γ_1 for silver used was 1.62×10^{-9} mol/cm^2, with the atomic radius being 1.60 Å [21].

Table 2: w_2 and χ values for SWV silver deposition on platinum in aqueous HNO_3 with 0.027 M $AgNO_3$ at 23.1°C using a silver wire pseudo reference

	$\Delta t^{1/2}$/s$^{1/2}$	f/Hz	w_2/V	χ
IR = 6.52 Ω (90%)	2.24	0.1	0.0202	142
IR = 6.88 Ω (95%)	2.24	0.1	0.0195	142
IR = 7.23 Ω (99.9%)	1.58	0.2	0.0193	101

4.2 Ni Deposition on W

To get a value for the diffusion coefficient of Ni^{2+} in molten LiCl, a series of cyclic voltammetry measurements were performed at varying scan rates and the peak current and peak potential were recorded for the reduction of nickel. Figure 5 shows the resulting voltammogram for four scan rates. As seen in this figure the reduction peak of nickel was found to be approximately at -0.05 V compared to a tungsten wire pseudo reference.

To calculate the diffusion coefficient, the range in which this deposition reaction is reversible must first be determined. Figures 6 and 7 show the results of this analysis. As stated previously, Equation (13) provides criteria for determining reversibility: the peak current varying linearly with the square root of the scan rate and the peak potential being independent of the log of scan

 https://doi.org/10.1016/j.electacta.2022.140220

rate. By comparing the two figures below, the reduction of nickel under these conditions is identified to be reversible through the entire range (0.05 to 2 V/s) of measurements taken.

By fitting a linear trendline through the data in Figure 6 and setting the intercept equal to zero, a resulting slope of 0.3408 A $s^{1/2}$ $V^{-1/2}$ is found. Using a value of 1.463 g/cm^3 for the density of LiCl at 701ºC [22] and 0.419 wt.% $NiCl_2$ in the bulk solution as measured by ICP-MS, a value for the bulk solution concentration of nickel ions (C_{ox}^*) was calculated to be 4.730×10^{-5} mol/cm^3. Using this value for C_{ox}^*, the slope from Figure 6, and Equation (13), the diffusion coefficient of Ni^{2+} ions in LiCl at 701ºC was found to be 3.612×10^{-4} cm^2/s. This value is greater than the value reported by Ghallali (2009) for Ni^{2+} in LiCl-KCl at 585ºC of 4.80×10^{-5} $\pm0.72\times10^{-5}$ cm^2/s [23], but is determined at a higher temperature. At 700°C in LiCl-NaCl (5:1 by mass), a diffusion coefficient for Mg^{2+} of 1.58×10^{-4} cm^2/s is reported by Zhang et al. [24]. Additionally, the diffusion coefficients of $2.4\text{-}3.4\times10^{-4}$ cm^2/s were reported for Sn^{2+} in pure molten LiCl at 625°C [25]. Based on these literature values, the calculated diffusion coefficient of Ni^{2+} is reasonable.

Similar to what was done with silver deposition on platinum, a series of square-wave voltammetry measurements were conducted at a range of frequencies and IR compensations to compare the accuracy of each model in calculating the number of electrons exchanged. Table 3 shows the step potential (ΔE_s) and amplitude (ΔE) that were applied compared to the values recommended by Equations (8) and (9). As shown by Table 3, the applied parameters are well within the recommended range.

 https://doi.org/10.1016/j.electacta.2022.140220

Table 3: Experimental and recommended step potential and amplitude potential for nickel deposition

	$\Delta E_s/V$	$\Delta E/V$
Recommended Range [13]	-0.00965 to -0.00168	0.034 to 0.197
Experimental Parameters	-0.005	0.1

Figure 8 shows a graph of the experimental data along with the curves predicted by the various models being tested. Three sets of measurements with IR compensation of 0.0%, 50% (0.061 Ω), and 85% (0.1037 Ω) were run. As seen in this figure, the differing amounts of IR compensation produced a wide range of results. With 85% IR compensation, the trend of the square-wave voltammetry measurements over the range of frequencies is most evident. At low $\Delta t^{1/2}$ (corresponding to high frequencies), the w_2 comes down sharply and nearly follows the curve of F&K Truncated before jumping back up and leveling out for a while. This dip (between values of $\Delta t^{1/2}$ from 0.04 to 0.08 $s^{1/2}$) is expected to be due to nucleation effects. The data then levels off between values of $\Delta t^{1/2}$ from 0.13 to 0.16 $s^{1/2}$ before rising again due to surface area growth, natural convection, and/or radial diffusion effects. Figure 9 shows an example of an SWV measurement under these conditions. In this figure it can be clearly seen that at a frequency of 0.8 Hz (corresponding to a $\Delta t^{1/2}$ of 0.79 $s^{1/2}$), the back half (more negative) side of the peak is distorted by higher magnitude (more negative) currents, where it otherwise would be expected to decay to near zero (see Figure 1). Due to surface area growth, nucleation effects, and other non-idealities affecting shorter and longer pulse times, the data points in the plateau between 0.09 $s^{1/2}$ and 0.16 $s^{1/2}$ are believed to best represent the w_2 and the last of these points will be used to determine the number of electrons calculated later. Since it is more difficult to see these details

 https://doi.org/10.1016/j.electacta.2022.140220

in the curves of 0.0% and 50% IR compensation, the lowest value of w_2 in the range of $\Delta t^{1/2}$ from 0.09 to 0.16 $s^{1/2}$ will be used to calculate the number of electrons exchanged.

In Figure 8 it may be seen that within the range of 0.13 to 0.16 $s^{1/2}$, the Fatouros and Krulic's full model follows the experimental data for 85% IR compensation most closely followed by their truncated model and then the IR-compensated Fatouros and Krulic model. It should be noted that for IR compensations of 50% and 85% there is a region that appears to best fit the Barker model, but this region is subject to surface area growth and is not believed to be an accurate representation of the system. It should also be noted that while the F&K models fit the data well for 85% and 50% IR compensations, the data for 0% IR compensation is very far from the model. The exact reason for the discrepancy between the model is not known, but possible explanations may be error in estimating Γ_1, double-layer charging and/or nucleation effects.

To determine the timescale of nucleation effects on the deposition of nickel onto tungsten, the forward current in square-wave voltammetry versus the pulse duration (Δt) is plotted as seen in Figure 10. In this figure, the forward current is plotted for two potentials: -0.087 V and -0.117 V. These two curves resemble chronoamperograms depicting the nucleation effects on the deposition of nickel. For both curves the current rises at 1 ms, reaches a peak around 1.7 ms, and then decreases momentarily before rising asymptotically in the 5-10 ms region. This behavior is characteristic of nucleation [26–29] and tells us that we can expect to see nucleation affects when the current is sampled in a time frame on the order of milliseconds. This is further supported by the fact that at both -0.087 V and -0.117 V the backward current is still positive (i.e., oxidizing).

 https://doi.org/10.1016/j.electacta.2022.140220

Table 4 shows each value selected for w_2 along with their associated χ values. The Γ_1 for nickel used was 2.28×10^{-9} mol/cm^2, with the atomic radius being 1.35 Å [21]. To determine if the tungsten rod may be approximated as a planar electrode, Equation (12) was used. Using this relationship, the lowest frequency to approximate planar electrode behavior within 5% error is 11 Hz. Thus, all of the values for w_2 in Table 4 meet the condition in Equation (12).

Table 4: w_2 and χ values for SWV nickel deposition on tungsten in molten $NiCl_2$(0.419 wt.%)-LiCl at 701°C using a tungsten wire pseudo reference

	$\Delta t^{1/2}$/s$^{1/2}$	f/Hz	w_2/V	χ
IR = 0.0 Ω (0%)	0.158	20	0.0654	62.4
IR = 0.061 Ω (50%)	0.129	30	0.0592	50.9
IR = 0.1037 Ω (85%)	0.158	20	0.0511	62.4

4.3 La Deposition on W

The diffusion coefficient for La^{3+} in molten LiCl was obtained in the same manner as that for Ni^{2+}. Figure 11 shows a voltammogram overlay of four scan rates used in obtaining this data set. As seen in this figure the reduction peak of lanthanum was identified to be at approximately -1.6 V compared to a tungsten wire pseudo reference. Figures 12 and 13 show the results of the peak current and potential as a function of scan rate for lanthanum deposition onto tungsten during cyclic voltammetry. By comparing these figures, the reversible region for lanthanum deposition onto tungsten under these conditions is identified to be through the entire range (0.05 to 2 V/s) of measurements taken.

 https://doi.org/10.1016/j.electacta.2022.140220

The slope of the deposition peak current versus the square root of the scan rate plot in Figure 12 was determined to be 0.3358 A $V^{-1/2}$ $s^{1/2}$. Using a value of 1.464 g/cm^3 for the density of LiCl at 698ºC [22] and a composition of 0.4332 wt.% $LaCl_3$ in the bulk solution as measured by ICP-MS, the value for the bulk solution concentration of lanthanum ions (C_{ox}^*) was calculated to be 2.586×10^{-5} mol/cm^3. Using this value for C_{ox}^*, the slope from Figure 12, and Equation (13), the diffusion coefficient of La^{3+} ions in LiCl at 698ºC was found to be 3.42×10^{-4} cm^2/s. This is greater than the values found by Castrillejo et al. in LiCl-KCl at a lower temperature of 450ºC of 1.15×10^{-5} cm^2/s and 1.17×10^{-5} cm^2/s [10]. It also compares well to the diffusion coefficient value of Ni^{2+} and the other values from the literature presented with nickel results earlier in this work.

To study the effect of nucleation overpotential on the shape of the square-wave voltammetry deposition peaks, a series of chronoamperometry measurements were conducted. Figure 14 shows the results of one of these measurements. As seen in this figure, the current initially rises sharply, then reaches a maximum (between 0.65 to 0.75 ms) which represents the timeframe that the current is affected by nucleation [29,30]. From this analysis, it was determined that the timescale for nucleation effects in lanthanum deposition is on the order of 0.7 ms. In square-wave voltammetry this would correspond to a Δt of approximately 0.2-2 ms ($\Delta t^{1/2}$ of 14 to 44 ms) or a frequency of approximately 2500-250 Hz. This corresponds well to the dip in Figure 15, supporting the hypothesis that the cause of the dip is nucleation. Further work is necessary to conclusively determine that this is the case. It should be noted that the deposition potential of lanthanum varies between approximately -1.6 V in Figure 11 and -1.5 V in Figure 14. This is

 https://doi.org/10.1016/j.electacta.2022.140220

likely due to variance in the tungsten wire pseudo-reference electrode over the course of a day of experimentation.

To test the validity of each model in calculating the number of electrons exchanged, a series of square-wave voltammetry measurements were performed in the same manner as that for silver and nickel.

Table 5 shows the step potential (ΔE_s) and amplitude (ΔE) applied in comparison to the values recommended by Equations (8) and (9). As shown by Table 5, the measurements were performed well within the recommended range. Again, three sets of measurements were made at differing amount of IR compositions: 0%, 50% (0.059 Ω), and 85% (0.1003 Ω).

Table 5: Experimental and recommended step potential and amplitude potential for lanthanum deposition

	$\Delta E_s/V$	$\Delta E/V$
Recommended Range [13]	-0.00642 to -0.00112	0.022 to 0.131
Experimental Parameters	-0.003	0.08

Figure 15 shows the results of the square-wave voltammetry tests for lanthanum deposition as they compare to the models being tested. Similar to what was seen with nickel deposition, the variance in IR compensation produced a wide range of results. Using the same logic as applied to the nickel deposition results, it is suspected that the least distorted values for w_2 are found in the range of $\Delta t^{1/2}$ from 0.13 to 0.19 $s^{1/2}$. Once again Fatouros and Krulic's model in the range of

 https://doi.org/10.1016/j.electacta.2022.140220

0.13 to 0.19 $s^{1/2}$ seems to follow the data the best for the data with an IR compensation of 85%, followed by their truncated model and then the IR-compensated version that was proposed in this work. The values selected for w_2 along with their associated χ values are given in Table 6. The Γ_1 for lanthanum used was 1.09×10^{-9} mol/cm^2, with the atomic radius being 1.95 Å [21].

Table 6: w_2 and χ values for SWV lanthanum deposition on tungsten in molten $LaCl_3$(0.433 wt.%)-LiCl at 698°C using a tungsten wire pseudo reference

	$\Delta t^{1/2}/s^{1/2}$	f/Hz	w_2/V	χ
IR = 0.0 Ω (0%)	0.183	15	0.0419	79.9
IR = 0.059 Ω (50%)	0.183	15	0.0299	79.9
IR = 0.1003 Ω (85%)	0.183	15	0.0273	79.9

Using Equation (12), the lowest frequency is 11 Hz at which the planar electrode approximation could be applied to the tungsten WE rod with less than 5% error. Thus, all of the values for w_2 in Table 6 satisfy the condition of a planar electrode without introducing significant error.

4.4 Comparison of Models to Calculate *n*

Using the w_2 values obtained for the deposition of silver on platinum and nickel and lanthanum on tungsten, the number of electrons exchanged was predicted by each of equations (1), (2), (5), (10), and (11). It is expected that 1, 2, and 3 electrons are exchanged for Ag, Ni, and La, respectively, based on their cyclic voltammograms and previous studies [13,26,31]. Table 7 shows the results of these calculations along with their associated error. Similar to what was seen in Figures 4, 8 and 15, it can be seen in Table 7 that the full model by Fatouros and Krulic (F&K) performs far better than both Barker and Aoki et al., supporting the claim that these theories only work for soluble-soluble reactions and are "right by chance only" [13]. This claim

 https://doi.org/10.1016/j.electacta.2022.140220

is further supported by Ghosh et al. in which Barker's model is reported to work for soluble-soluble reactions but not for soluble-insoluble reactions [3]. In the case of Aoki et al., the model did not converge well for the nickel or lanthanum reactions.

Table 7: Comparison of the number of electrons calculated by each model and their associated error relative to the expected number of electrons exchanged (n=1 for Ag, n = 2 for Ni, n = 3 for La)

	Barker		Aoki et al.		F&K		F&K Truncated		IR-F&K	
Trial	**n**	**Error**	**n**	**Error**	**n**	**Error**	**n**	**Error**	**n**	**Error**
Ag 90%	2.22	122%	1.14	14%	1.48	48%	0.92	8%	0.88	12%
Ag 95%	2.30	130%	1.14	14%	1.22	22%	0.93	7%	0.92	8%
Ag 99%	2.33	133%	1.14	14%	1.04	4%	0.93	7%	0.93	7%
Ni 0%	2.26	13%	3.74	87%	1.27	37%	1.18	41%	0.90	55%
Ni 50%	2.50	25%	3.74	87%	1.73	13%	1.19	41%	0.99	50%
Ni 85%	2.89	45%	3.74	87%	1.50	25%	1.21	40%	1.15	43%
La 0%	3.52	17%	4.64	55%	1.75	42%	1.91	36%	1.40	53%
La 50%	4.93	64%	4.75	58%	2.48	17%	2.66	11%	1.96	35%
La 85%	5.39	80%	4.66	55%	4.54	51%	2.32	23%	2.15	28%

As seen in Table 7, the error in the F&K model decreases with increasing IR compensation with the exception of Ni 85% and La 85%. This could possibly be due to overcompensation, may be experimental noise, or error in the estimated Γ_1. The large error associated with La 85% is best explained by Figure 16, where the limits of the F&K model are compared with the F&K

 https://doi.org/10.1016/j.electacta.2022.140220

Truncated model. This figure presents the w_2 predicted by both models as a function of n at the experimental conditions of La 85%. Also shown in this figure is the experimentally observed value for w_2, represented by the dashed line. As shown in Figure 16, both the F&K and F&K Truncated models predict a quadratic relationship with n [13]. Thus, when using a numerical solver, the final prediction for n depends greatly on the guess value you start with. It should also be noted that for values of n above the minimum of either curve, the slope becomes shallower which would result in greater error for the calculated number of electrons if the solver converged to the upper solution (for example, for F&K Truncated and La 85% the solver converges on n = 28.5). Any experimentally observed value of w_2 below the absolute minimum of the model will result in the n correlated with the model minimum. This is the case for the full F&K model with La 85% as seen in Figure 16, where the error of the model is minimized for n = 4.54. This explains why the F&K model has such a large error in calculating n for La 85% even though the experimentally observed value for w_2 is only 13% away from 30.9 mV, the value that converges exactly to n = 3.

As seen in Table 7, the IR-F&K model introduced at most 5% additional error from the F&K Truncated model where the ohmic drop is well-compensated (above 85% IR compensation). Through each set of experiments with silver, nickel, and lanthanum, it was observed that the IR-compensated Fatouros and Krulic model consistently underpredicts the number of electrons exchanged. Thus, with great consistency, it is suggested that the IR-compensated Fatouros and Krulic model can correctly predict the number of electrons exchanged when applying a ceiling function and rounding up to the nearest integer under the strict constraint of well-compensated ohmic drop.

 https://doi.org/10.1016/j.electacta.2022.140220

Alternatively, the underprediction may be due to effects not captured in the model. Since the F&K Truncated model is a linear approximation, the data gathered in this paper may be used to regress a new, experimentally observed linear fit. When doing this across all data sets for Ag, Ni, and La the following fit is obtained:

$$W_2 = 0.91 + 0.32\rho \quad (16)$$

Where the error on the intercept and slope are 0.19 and 0.15 respectively based on a 95% confidence interval. This would simplify to $W_2 = 0.91$ in the well-compensated case. Using the value of 0.91 in the IR-F&K model results in n = 1.06 for Ag at 90% IR compensation, n = 1.49 for Ni at 85% IR compensation and n = 2.79 for La at 85% IR compensation. While these initial results are promising, theoretical backing for the change from 0.7 in Equation (10) to 0.91 in Equation (12) is needed as well as more data to improve statistical certainty.

5. Conclusion

Models by Baker, Aoki et al., and Fatouros and Krulic are compared in their accuracy to calculate the number of electrons exchanged in metal deposition reactions. It is found that the full Fatouros and Krulic model most frequently provides the most accurate predictions of the number of electrons exchanged in the cases of one, two, and three-electron exchange reactions. Both models by Barker and Aoki et al. calculated the incorrect number of electrons exchanged for most of the experimental data sets, supporting the claim that they are meant for reactions in which both the oxidized and reduced species are soluble in either the electrode or the electrolyte and are only right by coincidence in the case of soluble-insoluble reactions.

A proposed modification to Fatouros and Krulic's model which is called the IR-compensated Fatouros and Krulic model proved to introduce minimal additional error (0-5%) under the

 https://doi.org/10.1016/j.electacta.2022.140220

constraint of well-compensated ohmic drop. It is suggested that this method is used for rapid determination of the number of electrons exchanged for unknown metal deposition reactions where there is insufficient information (e.g., unknown concentration) to use the more accurate and detailed models proposed by Fatouros and Krulic. The IR-compensated Fatouros and Krulic model correctly and reliably predicts the number of electrons exchanged when rounded up to the next integer. Since this method only requires a known temperature and does not require information on the concentration of the oxidized species, its diffusion coefficient, or any other information specific to the reacting species, it may be used in conjunction with the reduction potential to help identify unknown contaminants in aqueous and molten salt solutions in real time.

Furthermore, it was observed that w_2 departs from the trend predicted by Fatouros and Krulic, particularly in molten salt media. This departure at frequencies on the order of hundreds of hertz is postulated to be due to nucleation phenomena. At low frequencies, the departure is likely due to surface area growth, radial diffusion and/or natural convection. New coefficients were regressed for the Truncated Fatouros and Krulic model based on the observed experimental peak widths and uncompensated resistance. Future work on this topic could include investigating the effect of nucleation on square wave voltammograms, further minimizing the effects of resistance, and testing the IR-compensated Fatouros and Krulic model against other systems and conditions to investigate the influence of concentrations, substrates, ionic media, and temperatures on the calculated number of electrons exchanged.

6. Acknowledgements

This work was supported by the Department of Chemical Engineering at Brigham Young University.

 https://doi.org/10.1016/j.electacta.2022.140220

References

[1] M.R. Bermejo, E. Barrado, A.M. Martínez, Y. Castrillejo, Electrodeposition of Lu on W and Al electrodes: Electrochemical formation of Lu–Al alloys and oxoacidity reactions of Lu(III) in the eutectic LiCl–KCl, J. Electroanal. Chem. 617 (2008) 85–100. https://doi.org/10.1016/j.jelechem.2008.01.017.

[2] M.R. Bermejo, J. Gómez, A.M. Martínez, E. Barrado, Y. Castrillejo, Electrochemistry of terbium in the eutectic LiCl–KCl, Electrochimica Acta. 53 (2008) 5106–5112. https://doi.org/10.1016/j.electacta.2008.02.058.

[3] S. Ghosh, S. Vandarkuzhali, P. Venkatesh, G. Seenivasan, T. Subramanian, B. Prabhakara Reddy, K. Nagarajan, Electrochemical studies on the redox behaviour of zirconium in molten LiCl–KCl eutectic, J. Electroanal. Chem. 627 (2009) 15–27. https://doi.org/10.1016/j.jelechem.2008.12.011.

[4] C. Hamel, P. Chamelot, P. Taxil, Neodymium(III) cathodic processes in molten fluorides, Electrochimica Acta. 49 (2004) 4467–4476. https://doi.org/10.1016/j.electacta.2004.05.003.

[5] C. Hamel, P. Chamelot, A. Laplace, E. Walle, O. Dugne, P. Taxil, Reduction process of uranium(IV) and uranium(III) in molten fluorides, Electrochimica Acta. 52 (2007) 3995–4003. https://doi.org/10.1016/j.electacta.2006.11.018.

[6] K. Serrano, P. Taxil, Electrochemical reduction of trivalent uranium ions in molten chlorides, (n.d.) 7.

[7] J. Serp, P. Chamelot, S. Fourcaudot, R.J.M. Konings, R. Malmbeck, C. Pernel, J.C. Poignet, J. Rebizant, J.-P. Glatz, Electrochemical behaviour of americium ions in LiCl–KCl eutectic melt, Electrochimica Acta. 51 (2006) 4024–4032. https://doi.org/10.1016/j.electacta.2005.11.016.

[8] P. Chamelot, B. Lafage, P. Taxil, Using square-wave voltammetry to monitor molten alkaline fluoride baths for electrodeposition of niobium, Electrochimica Acta. 43 (1998) 607–616. https://doi.org/10.1016/S0013-4686(97)00102-3.

[9] P. Chamelot, P. Taxil, B. Lafage, Voltammetric studies of tantalum electrodeposition baths, Electrochimica Acta. 39 (1994) 2571–2575. https://doi.org/10.1016/0013-4686(94)00262-2.

[10] Y. Castrillejo, M.R. Bermejo, A.M. Martínez, A. Díaz, Electrochemical behavior of lanthanum and yttrium ions in two molten chlorides with different oxoacidic properties: The eutectic LiCl-KCl and the equimolar mixture CaCl2-NaCl, J. Min. Metall. Sect. B Metall. 39 (2003) 109–135. https://doi.org/10.2298/JMMB0302109C.

[11] G.C. Barker, R.L. Faircloth, A.W. Gardner, Square wave polarography. Part IV. An introduction to the theoretical aspects of square wave polarography, (1956). https://www.osti.gov/biblio/4317989.

[12] K. Aoki, K. Tokuda, H. Matsuda, J. Osteryoung, Reversible square-wave voltammograms independence of electrode geometry, J. Electroanal. Chem. Interfacial Electrochem. 207 (1986) 25–39. https://doi.org/10.1016/0022-0728(86)87060-7.

[13] N. Fatouros, D. Krulic, Analysis of the square wave voltammetry for reversible metal deposition on a foreign substrate – Experimental study of silver deposition on gold, J. Electroanal. Chem. 706 (2013) 76–85. https://doi.org/10.1016/j.jelechem.2013.07.019.

[14] Louis. Ramaley, M.S. Krause, Theory of square wave voltammetry, Anal. Chem. 41 (1969) 1362–1365. https://doi.org/10.1021/ac60280a005.

[15] M.S. Krause, Louis. Ramaley, Analytical application of square wave voltammetry, Anal. Chem. 41 (1969) 1365–1369. https://doi.org/10.1021/ac60280a008.

[16] M.R. Bermejo, J. Gómez, J. Medina, A.M. Martínez, Y. Castrillejo, The electrochemistry of gadolinium in the eutectic LiCl–KCl on W and Al electrodes, J. Electroanal. Chem. 588 (2006) 253–266. https://doi.org/10.1016/j.jelechem.2005.12.031.
[17] A.J. Bard, L.R. Faulkner, Electrochemical methods: fundamentals and applications, 2nd ed, Wiley, New York, 2001.
[18] T. Berzins, P. Delahay, Oscillographic Polarographic Waves for the Reversible Deposition of Metals on Solid Electrodes, J. Am. Chem. Soc. 75 (1953) 555–559. https://doi.org/10.1021/ja01099a013.
[19] G.J. Hills, D.J. Schiffrin, J. Thompson, Monolayer Formation in the Reduction of Nickel and Silver Ions from the LiCl-KCl Eutectic, J. Electrochem. Soc. 120 (1973) 157. https://doi.org/10.1149/1.2403413.
[20] P.J. Masset, Thermogravimetric study of the dehydration reaction of LiCl·H2O, J. Therm. Anal. Calorim. 96 (2009) 439–441. https://doi.org/10.1007/s10973-008-9399-y.
[21] J.C. Slater, Atomic Radii in Crystals, J. Chem. Phys. 41 (1964) 3199–3204. https://doi.org/10.1063/1.1725697.
[22] G.J. Janz, Thermodynamic and transport properties for molten salts: correlation equations for critically evaluated density, surface tension, electrical conductance, and viscosity data, J. Phys. Chem. Ref. Data. 17 (1988).
[23] H. El Ghallali, H. Groult, A. Barhoun, K. Draoui, D. Krulic, F. Lantelme, Electrochemical synthesis of Ni–Sn alloys in molten LiCl–KCl, Electrochimica Acta. 54 (2009) 3152–3160. https://doi.org/10.1016/j.electacta.2008.11.051.
[24] X. Zhang, S. Jiao, S. Xiao, H.M. Zhu, Electrochemical Behavior of Magnesium and Aluminium Ions in Alkali Chloride Melt, Mater. Sci. Forum. 488–489 (2005) 811–814. https://doi.org/10.4028/www.scientific.net/MSF.488-489.811.
[25] Q. Xu, C. Schwandt, D.J. Fray, Electrochemical investigation of lithium and tin reduction at a graphite cathode in molten chlorides, J. Electroanal. Chem. 562 (2004) 15–21. https://doi.org/10.1016/j.jelechem.2003.07.032.
[26] H. Tang, B. Pesic, Electrochemical behavior of LaCl3 and morphology of La deposit on molybdenum substrate in molten LiCl–KCl eutectic salt, Electrochimica Acta. 119 (2014) 120–130. https://doi.org/10.1016/j.electacta.2013.11.148.
[27] H. Tang, B. Pesic, Electrochemistry and Electrocrystallization of Gadolinium on Mo Substrate in LiCl–KCl Eutectic Salts, J. Electrochem. Soc. 161 (2014) D429–D436. https://doi.org/10.1149/2.0371409jes.
[28] S.-P. Gou, I.-W. Sun, Electrodeposition behavior of nickel and nickel–zinc alloys from the zinc chloride-1-ethyl-3-methylimidazolium chloride low temperature molten salt, Electrochimica Acta. 53 (2008) 2538–2544. https://doi.org/10.1016/j.electacta.2007.10.039.
[29] M.M. Tylka, J.L. Willit, M.A. Williamson, Electrochemical Nucleation and Growth of Uranium and Plutonium from Molten Salts, J. Electrochem. Soc. 164 (2017) H5327–H5335. https://doi.org/10.1149/2.0471708jes.
[30] L. Heerman, A. Tarallo, Theory of the chronoamperometric transient for electrochemical nucleation with diffusion-controlled growth, J. Electroanal. Chem. 470 (1999) 70–76. https://doi.org/10.1016/S0022-0728(99)00221-1.
[31] D. Horvath, M.F. Simpson, Electrochemical Monitoring of Ni Corrosion Induced by Water in Eutectic LiCl-KCl, J. Electrochem. Soc. 165 (2018) C226–C233. https://doi.org/10.1149/2.0391805jes.

Figures

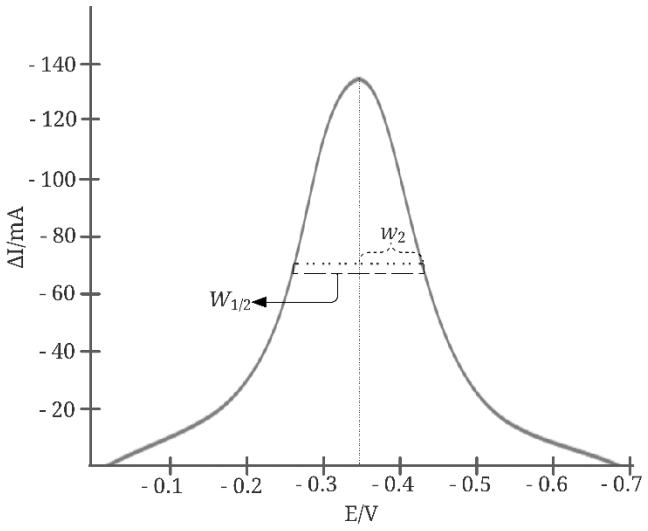

Figure 1: Illustration of the theoretical change in current (ΔI) versus potential (E) bell-shaped SWV deposition peak with the parameters w_2 and $W_{1/2}$ labeled

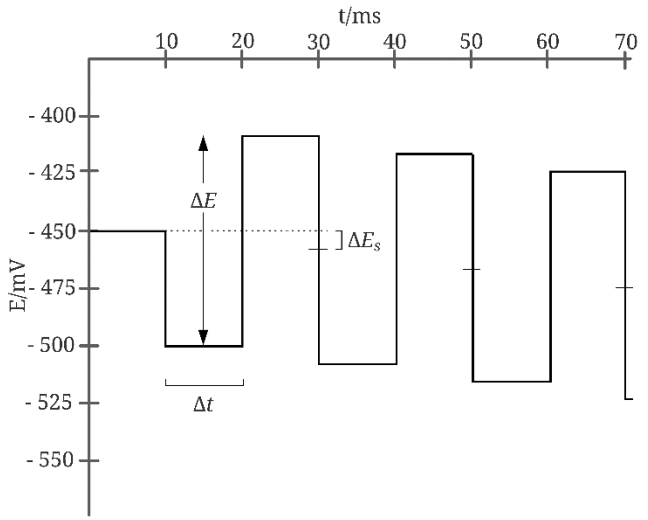

Figure 2: Illustration of the square wave waveform used in SWV with the parameters Δt, ΔE, and ΔE_s labeled

https://doi.org/10.1016/j.electacta.2022.140220

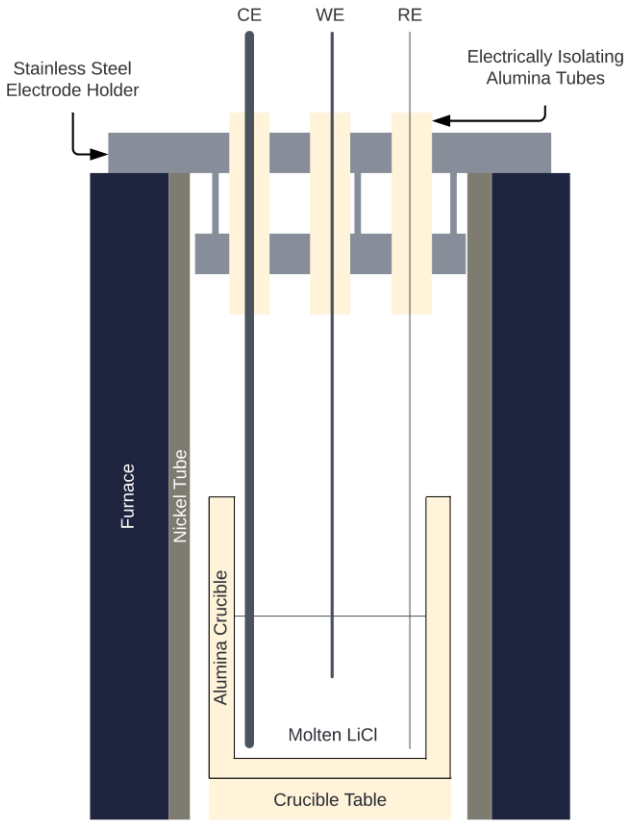

Figure 3: Diagram of experimental set up for all molten LiCl experiments. The WE was a 1.5 mm tungsten rod, the CE was a 3.175 mm tungsten rod, and the RE was a 1 mm tungsten wire quasi-reference electrode.

 https://doi.org/10.1016/j.electacta.2022.140220

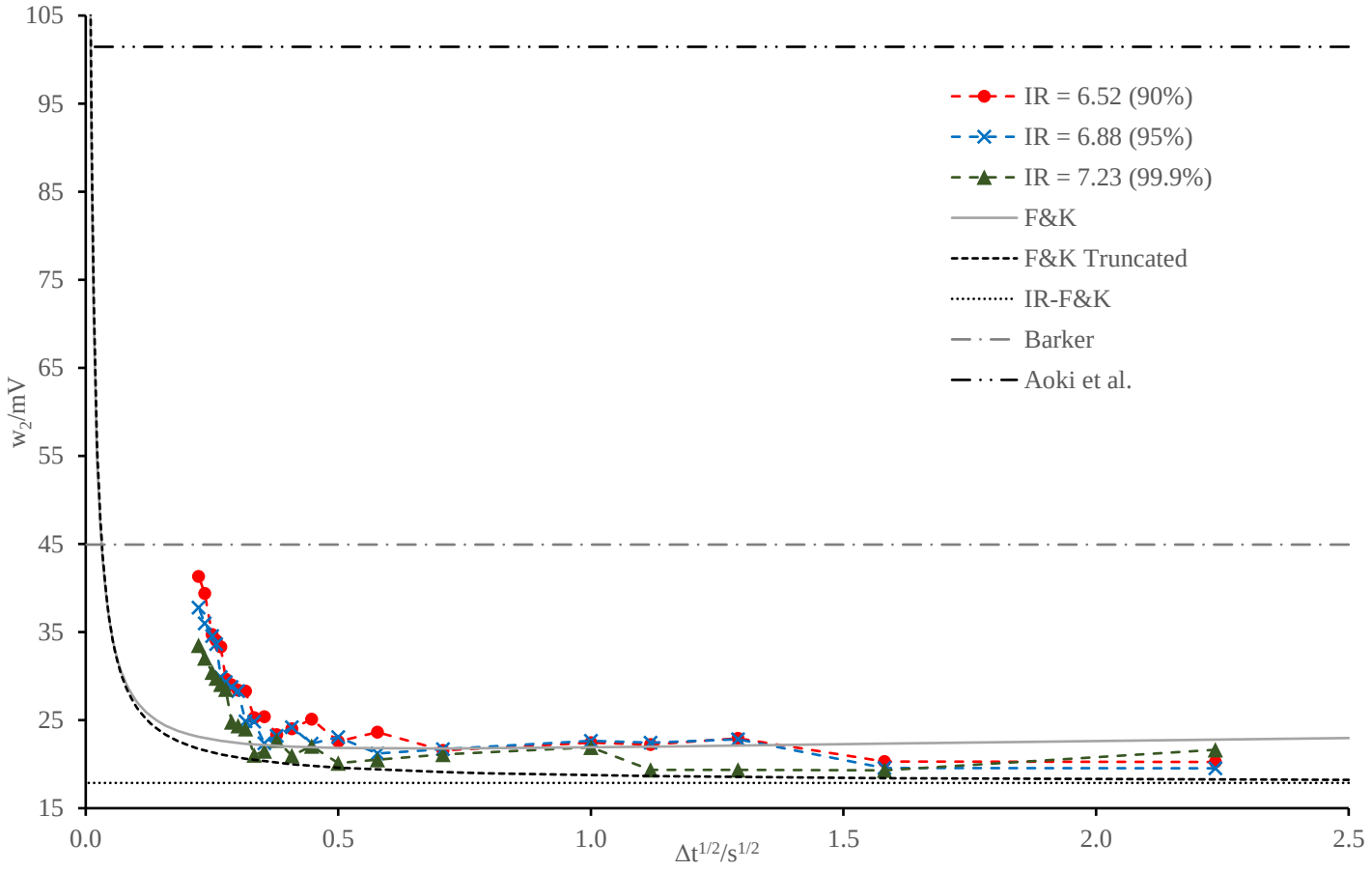

Figure 4: Graph of w_2 versus $\Delta t^{1/2}$ for silver deposition onto platinum in aqueous HNO_3 with 0.027 M $AgNO_3$ at 23.1°C using a silver wire pseudo reference. A value of 0.37 Ω was used for R_u in fitting the models

 https://doi.org/10.1016/j.electacta.2022.140220

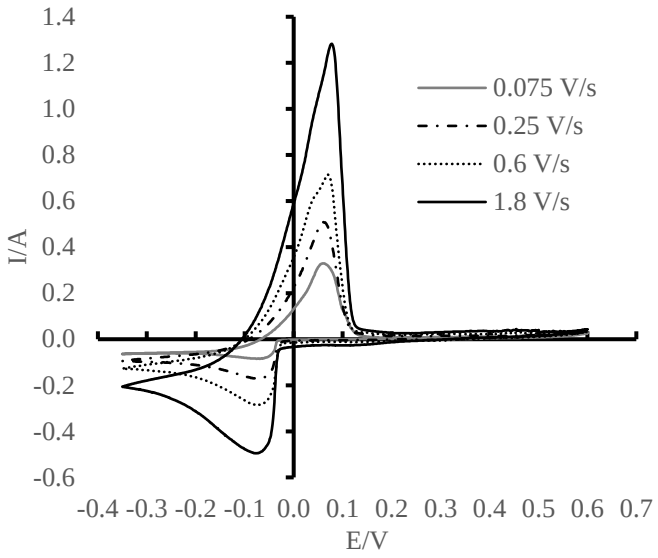

Figure 5: Overlay of four cyclic voltammograms at varying scan rates for the deposition of nickel onto tungsten in molten $NiCl_2$(0.419 wt.%)-LiCl at 701°C using a tungsten wire pseudo reference

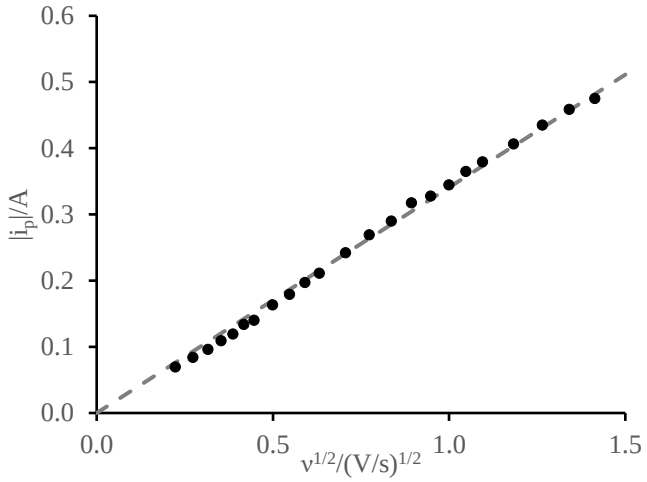

Figure 6: Peak current (i_p) of nickel deposition onto tungsten as a function of the square root of the scan rate $(v^{1/2})$ for cyclic voltammetry in molten $NiCl_2$(0.419 wt.%)-LiCl at 701°C using a tungsten wire pseudo reference

 https://doi.org/10.1016/j.electacta.2022.140220

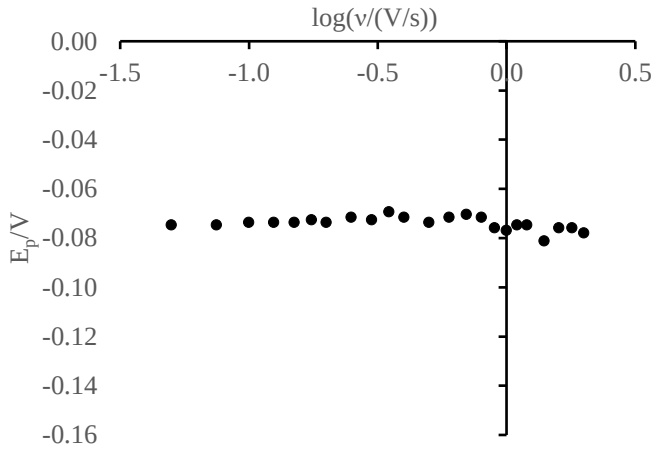

Figure 7: Peak potential (E_p) of nickel deposition onto tungsten as a function of the logarithm of the scan rate $(log(\nu))$ for cyclic voltammetry in molten $NiCl_2$(0.419 wt.%)-LiCl at 701°C using a tungsten wire pseudo reference

 https://doi.org/10.1016/j.electacta.2022.140220

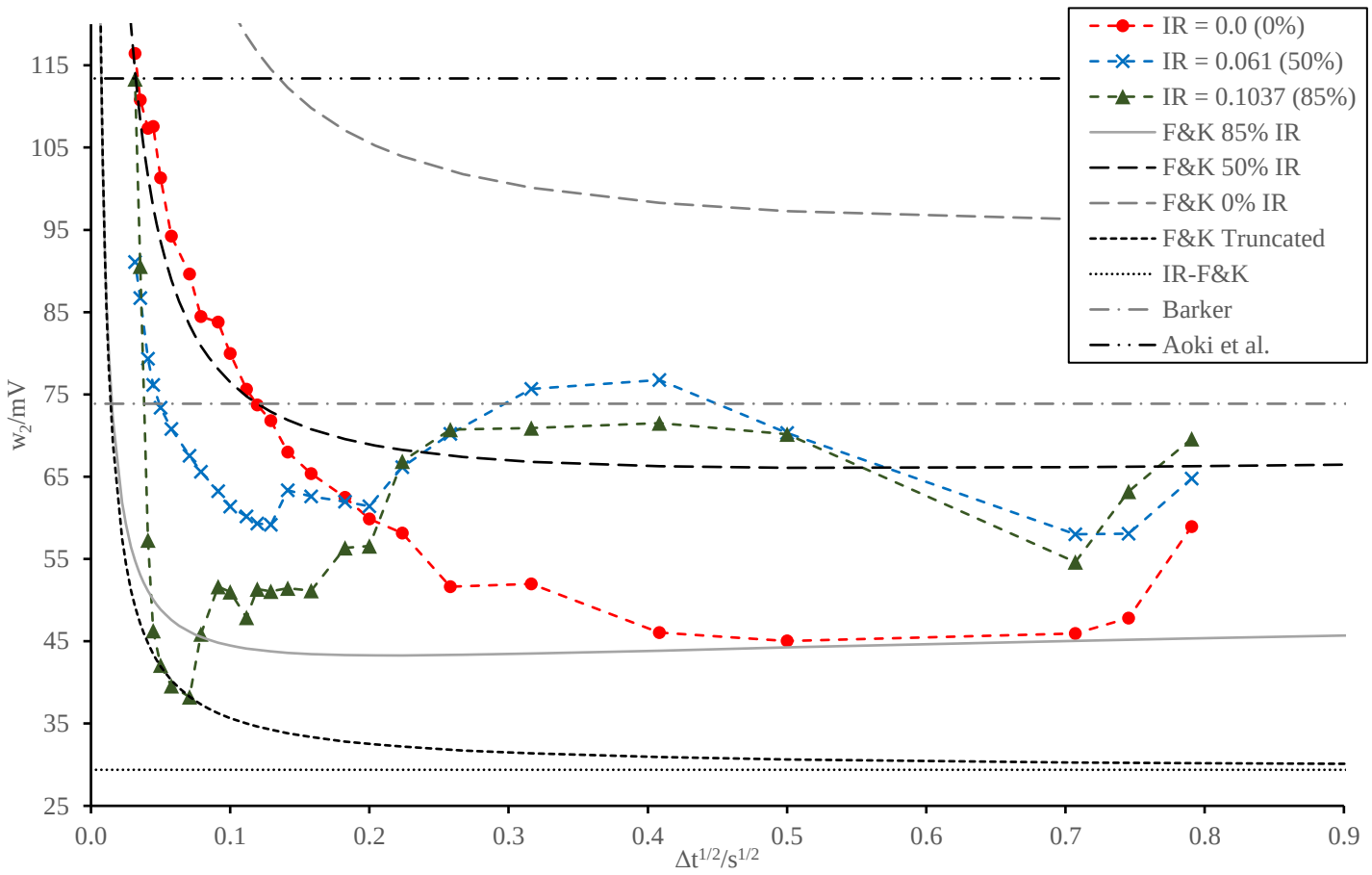

Figure 8: Graph of w_2 versus $\Delta t^{1/2}$ for nickel deposition onto tungsten in molten $NiCl_2$(0.419 wt.%)-LiCl at 701°C using a tungsten wire pseudo reference. A value of 0.0183 Ω was used for R_u when fitting the F&K Truncated model.

https://doi.org/10.1016/j.electacta.2022.140220

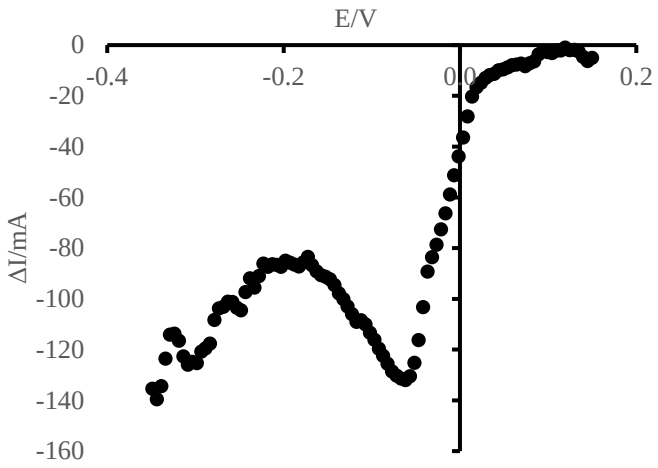

Figure 9: SWV peak for nickel deposition onto tungsten at a frequency of 0.8 Hz, where there is comparable distortion due to surface area growth, natural convection, and/or radial diffusion effects

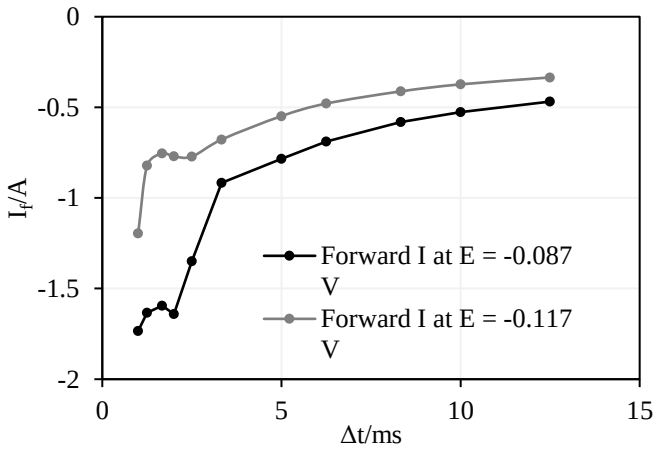

Figure 10: Forward current (I_f) recorded during nickel SWV measurements at different pulse durations

https://doi.org/10.1016/j.electacta.2022.140220

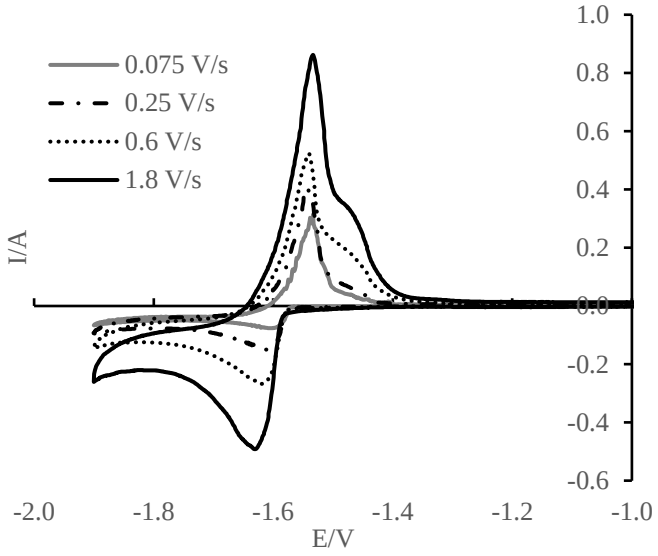

Figure 11: Overlay of four cyclic voltammograms at varying scan rates for the deposition of lanthanum onto tungsten in molten $LaCl_3$(0.433 wt.%)-LiCl at 698°C using a tungsten wire pseudo reference

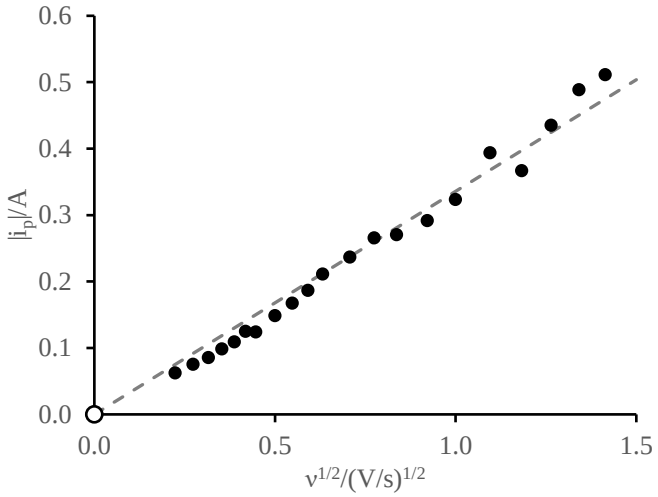

Figure 12: Peak current (i_p) of lanthanum deposition onto tungsten as a function of the square root of the scan rate ($\nu^{1/2}$) for cyclic voltammetry in molten $LaCl_3$(0.433 wt.%)-LiCl at 698°C using a tungsten wire pseudo reference

https://doi.org/10.1016/j.electacta.2022.140220

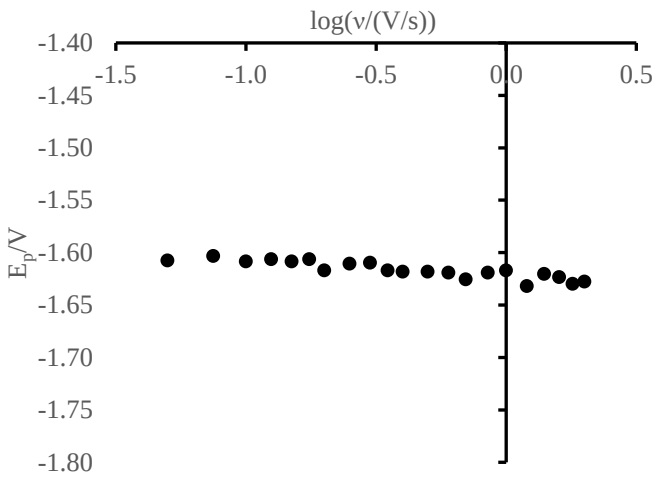

Figure 13: Peak potential (E_p) of lanthanum deposition onto tungsten as a function of the logarithm of the scan rate $(log(\nu))$ for cyclic voltammetry in molten $LaCl_3$(0.433 wt.%)-LiCl at 698°C using a tungsten wire pseudo reference

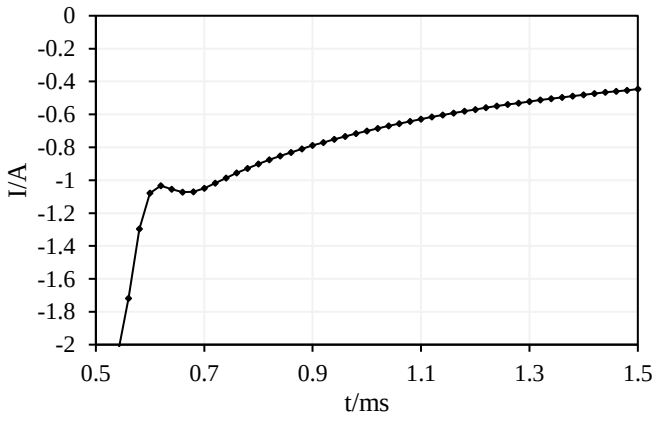

Figure 14: Chronoamperometry of lanthanum deposition onto tungsten at a potential of -1.5 V vs. W pseudo RE in molten $LaCl_3$(0.433 wt.%)-LiCl at 698°C using a tungsten wire pseudo reference

 https://doi.org/10.1016/j.electacta.2022.140220

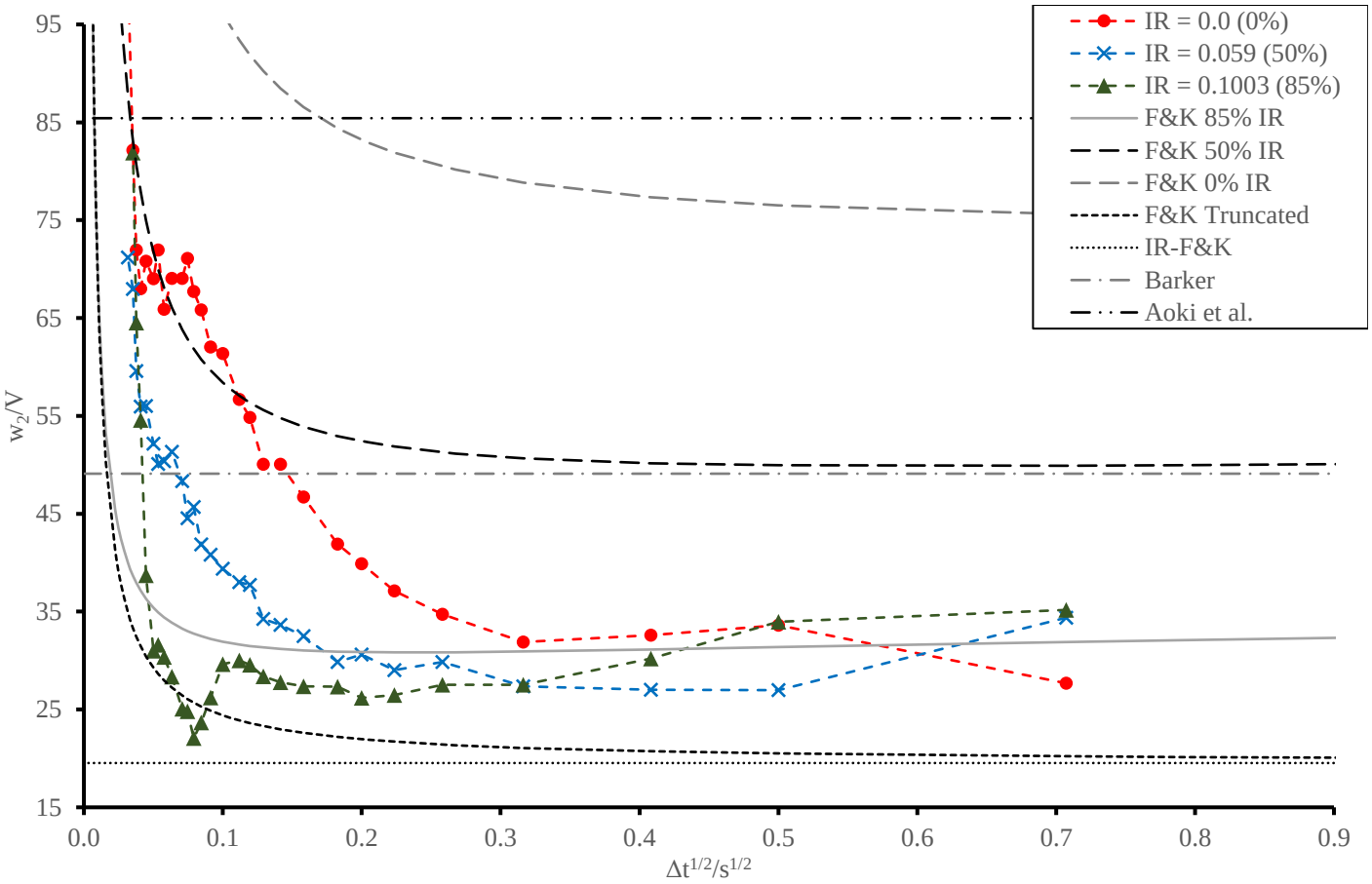

Figure 15: Graph of w_2 versus $\Delta t^{1/2}$ for lanthanum deposition onto tungsten in molten $LaCl_3$(0.433 wt.%)-LiCl at 698°C using a tungsten wire pseudo reference. A value of 0.0177 Ω was used for R_u in fitting the F&K Truncated model.

https://doi.org/10.1016/j.electacta.2022.140220

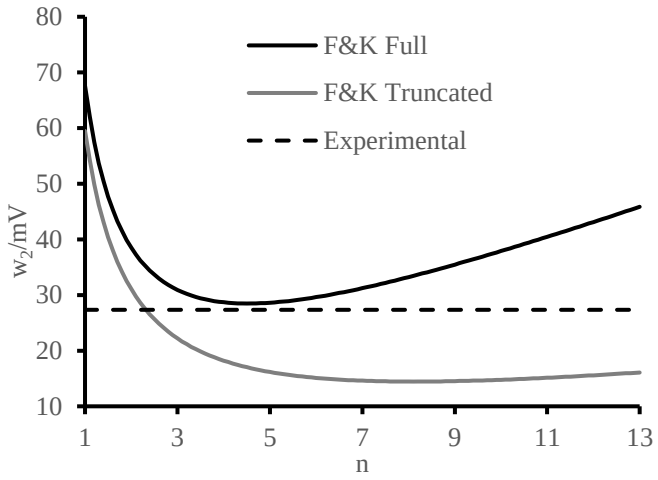

Figure 16: Graph of expected w_2 versus n as calculated by the F&K and F&K Truncated models for La 85% compared to the experimentally observed value for w_2

https://doi.org/10.1016/j.electacta.2022.140220